Separation and Purification Technology 363 (2025) 132047

Contents lists available at ScienceDirect

Separation and Purification Technology

journal homepage: www.elsevier.com/locate/seppur

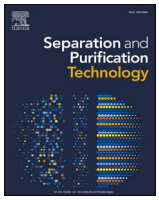

Novel nanofiltration composite membrane with a sandwich-structure of polyvinyl alcohol interlayer and Fe^{3+}-tannic acid polyamide layer for carbon source recovery

Xiujuan Hao [a,b,c], Yukai Hu [a,b], Rijian Quan [a,b], Xiayu Xu [a,b], Xin Liu [a,b], Yukun Li [a,b], Jiayu Tian [d,*]

[a] School of Civil Engineering, Inner Mongolia University of Technology, Hohhot, Inner Mongolia 010051, China
[b] Inner Mongolia Key Laboratory of Green Construction and Intelligent Operation and Maintenance of Civil Engineering, Hohhot, Inner Mongolia 010051, China
[c] School of Environment, Harbin Institute of Technology, Harbin 150090, China
[d] School of Civil and Transportation Engineering, Hebei University of Technology, Tianjin 300401, China

ARTICLE INFO

Editor: Junyong Zhu

Keywords:
Carbon source recovery
Sandwich structure
Surface modification
Thin-film composite membranes

ABSTRACT

Most wastewater treatment plants (WWTPs) encounter the problem of insufficient carbon sources. Particularly, the removal of organic pollutants is severely affected by carbon limitation and thus requires the use of external carbon sources in the secondary biological treatment process, which considerably increases operating costs. Even after the secondary treatment of high-concentration organic wastewater, the effluent still contains various organic substrates, such as low molecular weight organic acids and carbohydrates, etc., which can be used as carbon sources in the process of nitrogen and phosphorus removal. Effective separation and recovery of organic carbon sources in high-concentration organic wastewater are crucial to realize the resource utilization of organic carbon sources. In this study, a novel sandwich-structure thin-film composite (TFC) nanofiltration membrane was synthesized via chemically bonding polyvinyl alcohol (PVA) to form an interlayer and surface modification by Fe^{3+} and tannic acid (TA) chelating coordination on the polyamide (PA) layer. The design promoted the deposition of metal polyphenol networks on the PA layer, exposing more chelating sites while reducing the hydraulic resistance generated by deposition. The interlayer improved the permeability of the membrane, and the deposition of Fe–TA complexes enhanced membrane separation efficiency. Compared with the TFC-Fe membrane, the resulting membrane (PVA-TFC-Fe) showed a 56.42 % increase in permeability and enhanced rejection of inorganic salts and small-molecule organic carbon sources. Compared with the retention of the TFC-control membrane, that of PVA-TFC-Fe for small-molecule carbon sources, namely, acetic acid, propionic acid, and butyric acid, increased by 19.05 %, 17.34 %, and 15.67 %, respectively, and exhibited long-term operational stability.

1. Introduction

The amount of industrial organic wastewater discharged is increasing annually because of rapid industrialization. Large amounts of high-concentration organic wastewater increase the difficulty and cost of wastewater treatment [1]. Traditional wastewater treatment systems typically involve primary treatment, secondary treatment and advanced treatment [2]. Although secondary treatment (e.g., biological treatment) can effectively eliminate the organic matter in wastewater, it heavily relied on the supply of external energy and chemicals (external carbon sources), and such reliance considerably increases energy consumption and costs. The goal of wastewater treatment from pollution control to resource recovery represents a paradigm shift, it focuses not only on efficient contaminant removal, but also on the recovery and reuse of valuable resources, such as energy, water, chemicals, and heat [3].

In the wastewater treatment process, the carbon source is an indispensable substance and essential for effective denitrification and phosphorus removal [4,5]. Most wastewater treatment plants (WWTPs) have the problem of insufficient carbon sources [6]. Even after the high-

* Corresponding author.
E-mail address: tjy800112@126.com (J. Tian).

https://doi.org/10.1016/j.seppur.2025.132047
Received 23 December 2024; Received in revised form 28 January 2025; Accepted 9 February 2025
Available online 10 February 2025

concentration organic wastewater is treated by traditional water treatment processes, the concentration of organic matter in the secondary effluent still reaches hundreds of mg/L or more, and thus cannot meet relevant standards. This part of the effluent still contains many organic substrates that can be used as carbon sources, such as low-molecular-weight organic acids, carbohydrates, alkanes, alcohols, phenols, benzoates, and other benzene derivatives, etc.) [5,7]. These carbon sources can be reused in biological treatment processes as high-quality electron donors (e.g., volatile fatty acids [VFAs]) for microbial growth and metabolic utilization to solve the problem of insufficient carbon sources in WWTPs. Membrane technology, as an eco-friendly water treatment technology, has the characteristics of high separation efficiency, low energy consumption, sustainability, and no secondary pollution. Membrane technology not only plays a critical role in wastewater treatment but also promotes the efficient recovery and recycling of resources, thereby enhancing its application value in wastewater treatment [8]. It is recognized as an environmentally friendly and effective candidate method for resource recycling. Van Puffelen et al. [9] combined membrane water treatment with resource recovery, achieving a 66 % recovery of phosphorus and 34 % recovery of nitrogen from agricultural digestion wastewater using microfiltration (MF) and reverse osmosis (RO), etc. These recovered resources were reused as liquid organic fertilizers, replacing synthetic fertilizers. Under the dual demand for pollutant removal and resource recovery, nanofiltration (NF) membranes, with their precision in solute separation, have become an ideal choice [10]. Chu et al. [11] applied hollow fiber loose polyethersulfone NF membrane to the separation of dyes and salts, which exhibited 99.9 % Congo red rejection and over 93 % NaCl permeability in dye/salt mixture separation, indicating its great potential for resource recovery applications in textile wastewater treatment. This provides a sustainable solution for WWTPs.

NF is a low-pressure-driven membrane separation technology that has numerous advantages, including high separation efficiency, low energy consumption, absence of chemical alteration, and environmental friendly, and it has been widely used in wastewater treatment in recent years. The rejection performance of NF is between those of reverse osmosis and ultrafiltration, and its molecular weight cut-off (MWCO) is about 200–1,000 Da (Da) [12]. NF membranes in contact with an aqueous solution are usually charged because of the dissociation of surface functional groups or the adsorption of charged solutes. This feature makes NF membranes suitable for the selective separation of organic matter with different relative molecular masses and charges, these membranes can also be used in purification, concentration, and resource recovery in various industries [13]. NF membrane separation mechanisms include size sieving, the Donnan effect, and dielectric repulsion. To rationally utilize NF separation mechanisms in the effective separation of target solutes, researchers have successfully varied the membrane's surface properties, such as charge, hydrophilicity, and polarity, but this variation resulted in an enlarged membrane pore size and diminished solute separation performance [14,15]. Moreover, to enhance the separation performance of the membrane, some studies used modification approaches that require strict modification conditions, complicated reaction routes, or expensive raw materials [16,17], these approaches may cause membrane damage, and increase the overall cost. Thus, low-cost protocols must be established to develop PA-based membranes for the efficient separation of target solutes.

Surface modification, as a widely adopted strategy, aims to achieve effective separation of target solutes by tailoring the chemical properties and physical structure of membrane surfaces while minimizing the impact on the original structure of membranes [18]. Guo *et al.* introduced a hydrophilic polydopamine (PDA) coating on the membrane surface by surface coating, which effectively improved the removal of trace organic pollutants [19]. Ben *et al.* reported graft polymerization on the surface of NF membranes to enhance the rejection of endocrine-disrupting compounds (EDCs) [20]. Another study deposited a metal polyphenol network on the membrane surface, and the modified NF membrane exhibited more obvious rejection of organic micro-pollutants (OMPs) [21]. These studies have proved that surface modification increased separation performance and rejected various small-molecule pollutants. It was mainly attributed to the enhancement of the size exclusion effect due to the shrinking of pore size, which also increased the transport resistance of water molecule [21,22]. Recently, a growing number of researchers have focused on constructing highly permeable sandwich structures in the NF membrane to enhance the permeability of the NF membrane without sacrificing selectivity. This strategy involves integrating nanomaterials [23,24] or interfacial coating materials [25–27] into membrane structures. Surface modification strategies usually increase water transport resistance and inevitably reduce water permeability, possibly leading to higher energy consumption. Therefore, based on surface modification to enhance selectivity, the construction of sandwich structure could optimize the water transport pathway, mitigate the permeability loss caused by surface modification, and further improve the versatility of NF membrane in the water treatment process.

The selectivity of NF membrane separation is a key parameter affecting the recovery of resources from waste liquid resources, and interface modification strategies can effectively improve this performance. In this study, a novel sandwich-structure TFC-NF membrane was synthesized through chemically bonding PVA forming the interlayer and Fe–TA complex deposition on the surface of the PA layer. The sandwich-structure changed the interfacial polymerization reaction conditions, and the exposed proportion of carboxyl functional groups of the PA layer increased, which promoted the deposition of Fe–TA complex and further improved the membrane selectivity. Meanwhile, the sandwich-structure effectively mitigated the water permeability loss caused by Fe–TA complex deposition on the selective layer, thereby reducing the hydraulic resistance. To simulate the charged small-molecule organic carbon source in high-concentration organic wastewater, three kinds of VFAs, namely, acetic acid, propionic acid, and butyric acid, were utilized to represent the charged small-molecule organic carbon sources in high-concentration organic wastewater. The sandwich-structure TFC-NF membrane was applied to carbon source recovery. In addition, the separation performance of the sandwich-structure NF membrane was evaluated and the specific roles of the interlayer and the coating layer in the improvement of membrane performance were discussed. Based on the above work, the feasibility and potentiality of the sandwich-structure NF membrane for resource utilization of high-concentration organic wastewater have been demonstrated.

2. Materials and methods

2.1. Materials and chemicals

A substrate membrane made of polyethersulfone (MWCO = 10–15 kDa) was used as the support for the PA NF membrane, and it was provided by Beijing Separate Equipment Co., Ltd. (Beijing, China). Piperazine (PIP, 99 %), tannic acid (TA, 99 %), glutaraldehyde (GA, 50 wt% in H_2O), ferric chloride hexahydrate ($FeCl_3{\cdot}6H_2O$, 99 %), acetic acid (C-2, 99 %), propionic acid (C-3, 99 %), butyric acid (C-4, 99 %), and inorganic salts (including NaCl, $MgCl_2$, $MgSO_4$ and Na_2SO_4) were supplied by Shanghai Macklin Biochemical Co., Ltd., China. 1,3,5-Benzenetricarbonyl trichloride (TMC, 98 %), n-hexane (98 %), poly (vinyl alcohol) (PVA, Mw = 31,000–50,000), and polyethylene glycol (PEG-200, PEG-400, PEG-600, PEG-800, and PEG-1000) were purchased from Aladdin Reagent Company. Isopropyl alcohol (IPA, ≥99.9 %), sodium hydroxide (NaOH), HCl (36–38 wt%), and H_2SO_4 (95–98 wt%) were provided by China National Pharmaceutical Group Chemical Reagent Co., Ltd. (China).

2.2. Membrane preparation

2.2.1. Preparation of TFC-control membrane

The control TFC membrane was prepared using the traditional

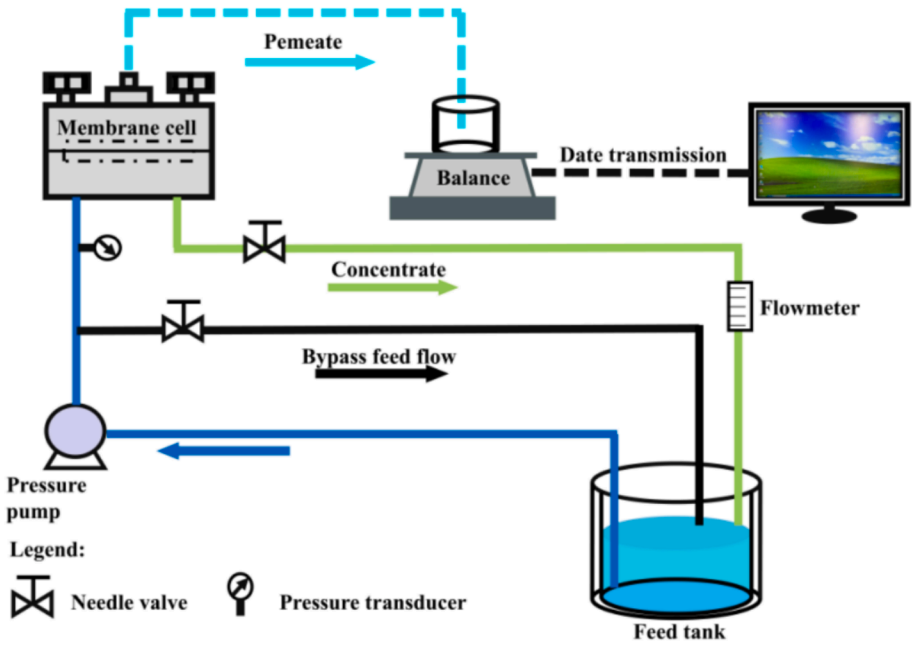

Fig. 1. Schematic of the NF cross-flow system.

interfacial polymerization method, and the substrate was rinsed and activated following a previously reported procedure [28], and then thoroughly washed with deionized (DI) water before use. First, the surface of the polyethersulfone (PES) substrate was immersed in an aqueous solution (containing 1.0 wt% PIP and 0.6 wt% NaOH) for 2 min. The excess solution was discarded, and the surface was dried with filter paper. Then, a 0.15 wt% trimesoyl chloride (TMC) organic (n-hexane) solution was poured onto the membrane surface and allowed to react for 30 s before being discarded. The membrane was drained for 2 min, then cured at 60 °C in an oven for 5 min to further polymerization. Finally, a PA layer was formed on the substrate, and the resulting membrane was named TFC-control.

2.2.2. Preparation of interlayer-TFC membrane

A certain concentration of PVA was dissolved in DI water at 95 °C under stirring. After complete dissolution, the solution was cooled to room temperature to obtain a PVA solution of the desired concentration. First, the PES substrate is positioned face up and immersed in an aqueous PVA solution for 5 min to remove excess liquid, and then air dried. Next, 1.0 wt% GA solution (containing 0.2 wt% HCl) is poured onto the membrane surface and left for 1 min, then poured off, and rinsed with DI water. Following the steps detailed in **Section 2.2.1**, the PVA-coated PES substrate formed a PA layer via interfacial polymerization, with the PVA concentration being optimized during fabrication. The resulting membrane, produced with the optimal ratio, was named PVA-TFC.

2.2.3. Preparation of TFC-surface modification membrane

The control membrane was fixed and the PA layer was upward. Then, a certain molar concentration of $FeCl_3{\cdot}6H_2O$ solution (35 ml) was prepared, and it was poured into the PA layer of the control membrane and gently shaken for 30 s. Then, TA solution (0.24 mM, 35 ml) was added and continued to shake for 60 s to fully react. The membrane formed with different Fe–TA molar ratios was evaluated, and the optimal-coated membrane was named TFC-Fe.

2.2.4. Preparation of sandwich-structure TFC membrane

Based on the formation of the interlayer, the sandwich-structure NF membrane was synthesized as follows: an optimal molar ratio Fe–TA polyphenol network was deposited on the top surface of the PVA-TFC. Briefly, the PVA-TFC membrane was exposed to 35 mL of $FeCl_3{\cdot}6H_2O$ solution at room temperature for 30 s. An equal volume of TA solution (0.24 mM) was introduced for a contact time of 60 s to form a stable Fe–TA coating. The resulting membrane was named PVA-TFC-Fe. The membrane was then washed with DI water and stored in DI water at 4 ℃ until testing.

2.3. Membrane characterization

The membrane samples used in the characterization were pre-vacuum dried at 30 °C for 24 h. The chemical structures of the membranes were analyzed using attenuated total reflectance-Fourier transform infrared spectroscopy (ATR-FTIR; Nicolet IS50Nicolet Continuum, Thermo Fisher Scientific, the USA) in the wavelength range of 400–4000 cm^{-1}. Surface elemental composition was determined through X-ray photoelectron spectroscopy (XPS; Thermo Fisher Scientific, ESCALAB 250Xi, the USA). Surface morphologies were examined with field emission scanning electron microscopy (FESEM; ZEISS, SUPRA 55, Germany). The membrane's surface charge properties were assessed using an electrokinetic analyzer (SurPASS, Anton Paar, Austria). Surface roughness was characterized by atomic force microscopy (AFM; Multimode 8, Bruker, Germany) with a scan size of 10 μm × 10 μm. Static water contact angles were determined using a contact angle goniometer (LSA 100, Lauda Scientific, Germany) using the sessile drop method (0.1 μL) at 25°C.

2.4. Test on membrane performance and pore size

The permeation and rejection performance of the membranes were evaluated using a laboratory-scale crossflow NF cell (CF016, Sterlitech, the USA). The schematic of the cross-flow system is shown in Fig. 1. Before conducting the membrane performance tests, the membrane samples were compacted under 6 bar pressure using DI water for 1 h to stabilize the membrane state. In the test, the applied pressure was 4 bar, and the water temperature was regulated at room temperature. Permeate weight data were monitored every 5 s by using a digital weight balance (LTB460i, ADAM, England) connected to a metering software for flux calculation. The permeate and the retentate were recirculated into the feed tank. Pure water permeance was calculated as equation (1):

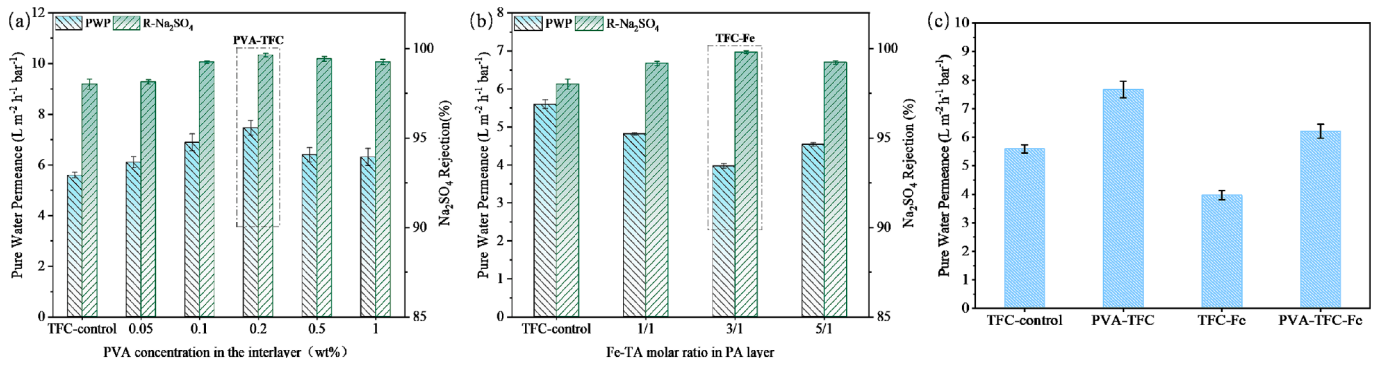

Fig. 2. (a) Effect of PVA concentration on the performance of the membrane. (b) Effect of Fe–TA molar ratio on the performance of the membrane. (c) Pure water flux of the membranes.

$$J = \frac{V}{A \times \Delta t \times \Delta P} \tag{1}$$

where J is the permeation flux (L $m^{-2}h^{-1}$ bar^{-1}), V is the volume of the permeate (L), A is the membrane area (m^2), Δt is the permeate collection interval (h), and ΔP is the *trans*-membrane pressure (bar).

Water solutions of inorganic salts (NaCl, $MgCl_2$, $MgSO_4$ or Na_2SO_4), and VFAs as small-molecule organic carbon sources were prepared as the feed water. The salt concentrations in both the feed and permeate solutions were measured using a conductivity meter (DDSJ-308F, Shanghai INESA Scientific Instrument, China). The concentration of VFAs in the feed and permeate was determined using a high-performance liquid chromatograph (HPLC-20A, Shimadzu, Japan) with a separating column (SUGAR SH1011, Shimadzu, Japan), a guard column (SH-G, Shimadzu, Japan), and a refractive index detector at the column temperature of 50 °C. The eluent of the 0.01 N H_2SO_4 solution had a constant rate of 1.0 mL min^{-1}. The rejection rate (R, %) was obtained through the equation (2):

$$R = \left(1 - \frac{C_p}{C_f}\right) \times 100\% \tag{2}$$

where C_f and C_p are the concentrations of the feed and permeate solutions, respectively.

The MWCO of the fabricated NF membranes was determined by measuring the rejection of PEG with varying molecular weights (200, 400, 600, 800, and 1000 Da) at a fixed rejection rate of 90 %. The concentration of the PEG solutions was measured using a visible spectrophotometer after a chromogenic reaction with 0.05 mol L^{-1} I_2 aqueous solution and 5.0 % $BaCl_2$ aqueous solution. The rejection of PEG was calculated using Eq. (2).

3. Results and discussion

3.1. Effect of PVA concentrations for interlayer

To understand the effect of interlayers on the performance of TFC membranes, different concentrations of PVA (0, 0.05, 0.1, 0.2, 0.5, and 1.0 wt%) were chemically bonded on PES substrate to form PVA interlayer, and their filtration performance was evaluated. As shown in Fig. 2**a**, The pure water flux and Na_2SO_4 rejection increased from 5.59 L $m^{-2}h^{-1}$ bar^{-1} and 98.02 % for the control membrane to 7.46 $m^{-2}h^{-1}$ bar^{-1} and 99.64 % for the optimized sandwich NF membrane at 0.2 wt% concentration of PVA, respectively, and there is no limitation between permeability and selectivity. This might be attributed to the strong hydrogen bonding between the PVA interlayer and the PIP monomer, resulting in changes in the properties of the NF membrane, including the enhancement of hydrophilicity, the reduction of the thickness of the PA layer, and the mitigation of the substrate gutter effect [29]. However, higher PVA concentration may result in the formation of a thicker interlayer, which may adversely affect the NF membrane performance. The permeability of the sandwich NF membrane showed a decreasing trend at 0.5–1 wt% concentration of PVA but still maintained high retention performance. Considering the high permeability and rejection performance, the concentration of PVA selected for the subsequent membrane preparation was 0.2 wt% (PVA-TFC).

3.2. Effect of Fe–TA molar ratio for PA layer

To explore the effect of the surface layer on membrane properties, different concentrations of $FeCl_3{\cdot}6H_2O$ solution (0.24, 0.72, and 1.2 mM) with TA solution (0.24 mM) were used to coat-modify TFC membranes. As shown in Fig. 2**b**, the Na_2SO_4 rejection increased from 98.02 % to 99.81 % when the Fe–TA molar ratio was increased from 0 to 3/1. This is attributed to the fact that the presence of the coating layer effectively narrows the MWCO of the TFC membranes (**Fig. S1**). However, the enhancement of separation performance limited the membrane permeability. As the Fe − TA molar ratio increased from 0 to 3/1, the pure water flux decreased from 5.59 L $m^{-2}h^{-1}$ bar^{-1} to 3.97 L $m^{-2}h^{-1}$ bar^{-1}, indicating that the surface Fe–TA addition ratio affects permeability. The decrease in water permeability is attributed to the Fe − TA film on the membrane surface, which increased resistance to water flow through the PA separation layer. This also limits its application in membrane materials. Furthermore, when the Fe–TA molar ratio increased to 5:1, the pure water flux showed an increase. The large proportion of Fe ions may have rapidly formed large aggregated particles in the bulk solution, resulting in the inability to achieve effective coating on the membrane surface [30]. Considering the best separation performance, the molar ratio of Fe–TA selected for the following membrane preparation was set to 3/1 (TFC-Fe).

3.3. Comparison of membrane permeability

As shown in Fig. 2**c**, the pure water fluxes of the TFC-control, PVA-TFC, TFC-Fe, and PVA-TFC-Fe membranes were 5.59, 7.46, 3.97, and 6.21 L $m^{-2}h^{-1}$ bar^{-1}, respectively. The water flux of the PVA-TFC membrane was significantly better than that of the TFC-control membrane, showing the advantages of interlayer structure in permeability. The TFC-Fe membrane experienced a reduced permeation flux during the filtration of the pure water, which could be attributed to the coated Fe–TA film coated on the membrane surface, which increased the resistance of water molecules through the PA separation layer, leading to a decline in water permeability. However, the PVA interlayer mitigated this phenomenon, resulting in an enhanced pure water flux for the PVA-TFC-Fe membrane [30]. This could be attributed to the introduction of the sandwich-structure affecting the interfacial polymerization reaction conditions, which was manifested in the generation of nanovoids inside the PA layer, and as the PA layer becomes thinner and rougher, the water transport distance becomes shorter and the filtration

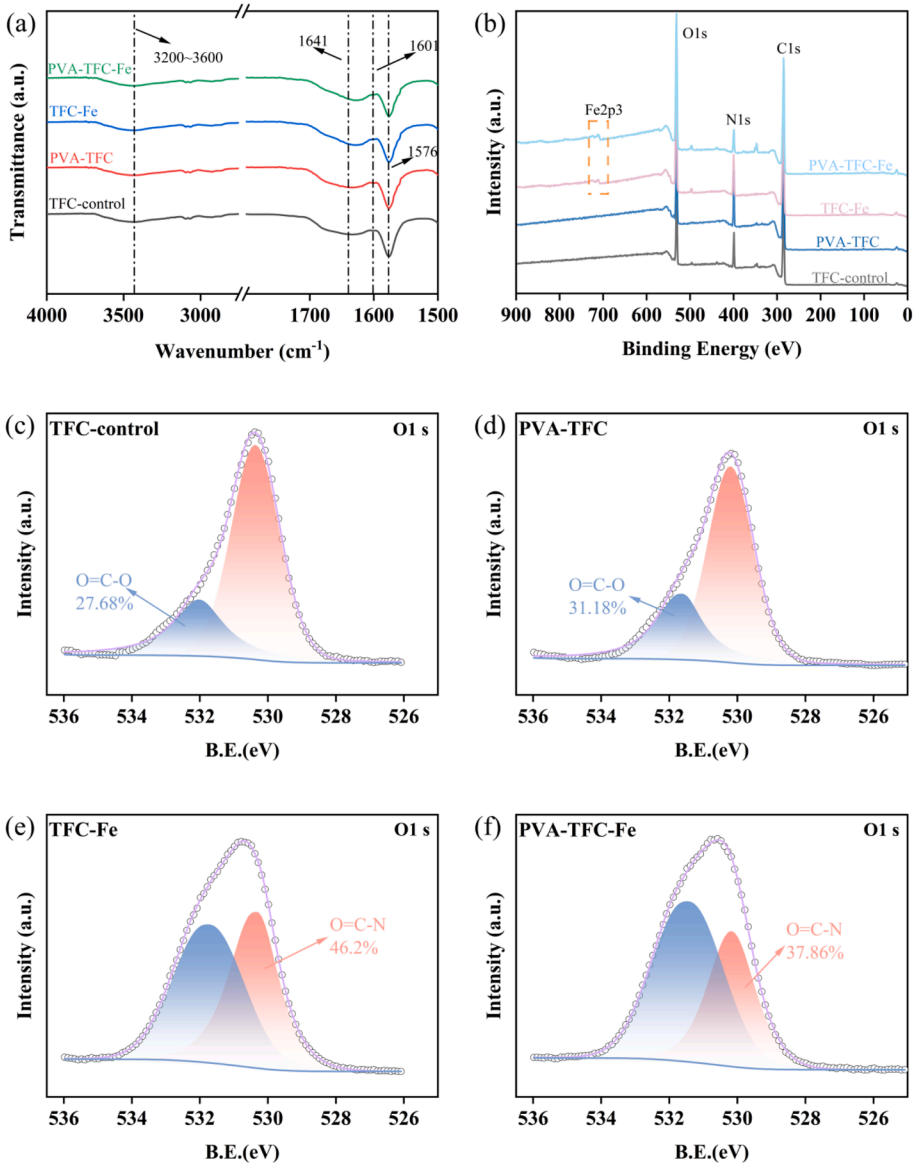

Fig. 3. Surface chemical characterization of the membranes: **(a)** FTIR, **(b)** XPS survey spectra, **(c)** O 1 s spectrum of TFC-control, **(d)** O 1 s spectrum of PVA-TFC, **(e)** O 1 s spectrum of TFC-Fe, and **(f)** O 1 s spectrum of PVA-TFC-Fe.

area increases [31–33]. In addition, the presence of the PVA interlayer improved the hydrophilicity of the substrate, which improved the water storage rate of the substrate, so that the substrate could resist the deformation of the substrate caused by the heat treatment process, maintained the water permeability of the substrate, and avoid the increase of water resistance [34].

3.4. Chemical properties of the membranes

The chemical composition of the membrane surface was further analyzed using ATR-FTIR. As shown in Fig. 3**a**, all membranes exhibited the characteristic peaks of polyamide: 1,576 cm^{-1} (the in-plane N–H bending vibrations of amide), 1,601 cm^{-1} (C–N tensile vibrations of amide), and the broad peak between 3,200 and 3,600 cm^{-1} (O–H bending vibration of the carboxylic acid group) [25,35]. Additionally, the characteristic peak at 1,641 cm^{-1}, related to the stretching vibration of O = C–O [36], of the Fe–TA coated membrane showed weakened peak intensity in comparison with the control. This is attributed to additional Fe^{3+} being introduced to the membrane surface because of the excellent ability to chelate carboxyl groups [37]. The bridging of Fe^{3+} between the TA and COOH groups on the membrane surface via a chemical bond, resulting in a weak peak intensity.

The surface elemental composition of the membranes was characterized by XPS, as shown in Fig. 3**b**. The appearance of Fe 2p3 peaks around 710 eV and the presence of Fe, together with a considerably increased signal of O and a reduced signal of N for the Fe–TA-coated membranes, verified the formation of the Fe–TA layer on the top of the TFC-control membrane's surface. This also demonstrated the changes in FTIR. The XPS spectra had an analysis depth of ~ 10 nm because the Fe–TA coating layer merely consisted of Fe, C, O, and H elements. The N element in the PA active layer could still be detected, which indirectly confirms that the thickness of the coating layer formed by the Fe–TA coordination complex was less than 10 nm [38]. Compared with the TFC-Fe membrane, the peak intensity of the Fe element in the PVA-TFC-Fe membrane was more significant, which could be attributed to the deposition of more Fe–TA coordination complexes on the membrane surface. The XPS spectra for O 1 s further revealed the change in membrane surface chemistry. As shown in Fig. 3**c-3f**, the binding energies of 531.2 eV and 532.6 eV were due to O = C–N and O = C–O, respectively [39]. It was observed that the content of the O = C–O

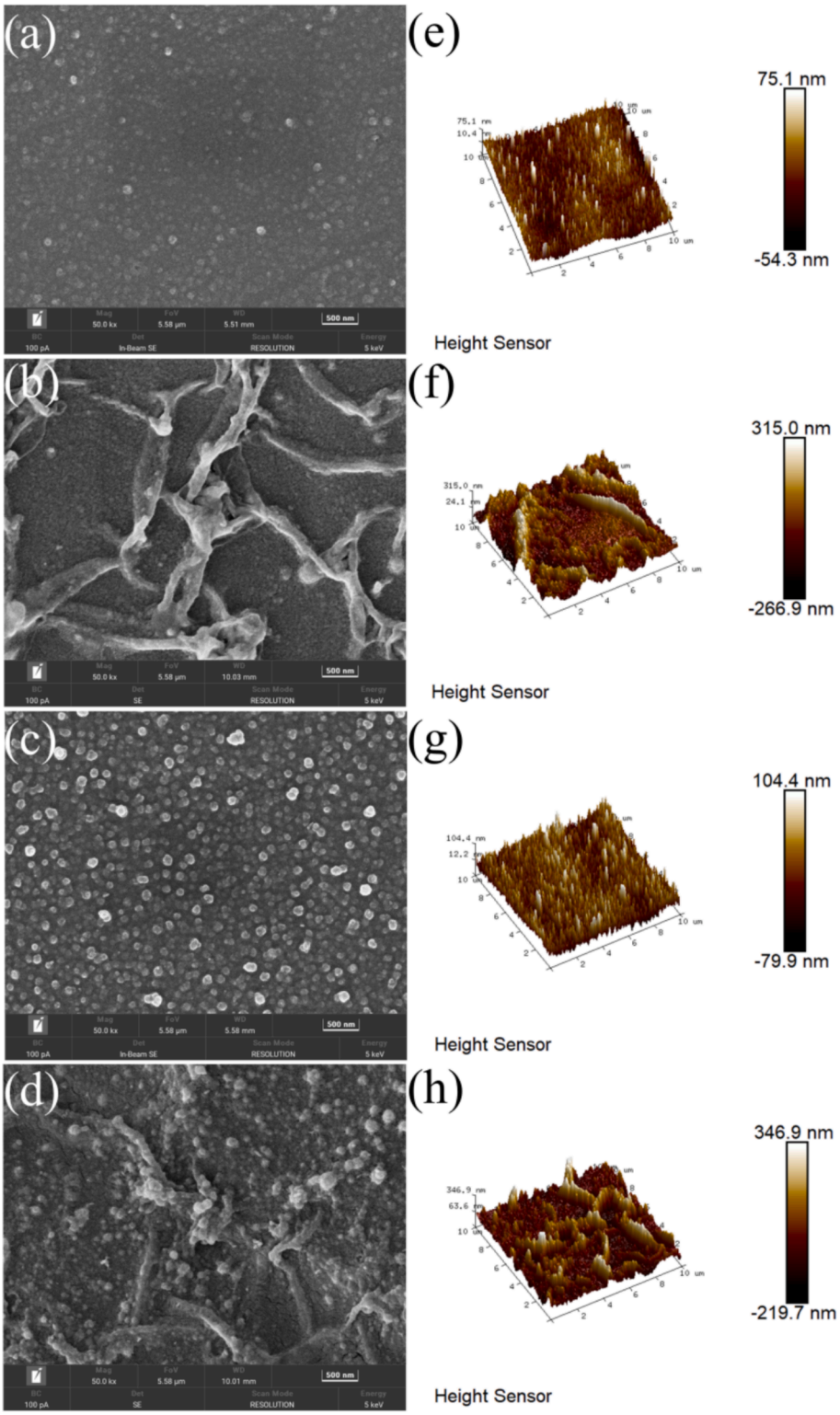

Fig. 4. Surface topographies of the NF membranes, SEM: (a) TFC-control, (b) PVA-TFC, (c) TFC-Fe, and (d) PVA-TFC-Fe; AFM: (e) TFC-control, (f) PVA-TFC, (g) TFC-Fe, and (h) PVA-TFC-Fe.

functional group increased from 27.68 % for the TFC-control membrane to 31.18 % for the PVA-TFC membrane. To clarify the reason for the increase in carboxyl content, the chemical composition of polyamide was analyzed by convolution of N1s spectra for the TFC-control and PVA-TFC membranes (Fig. S2). The N–H group was derived from the unreacted PIP and polyamide segments. The N–H content on the PVA-TFC membrane (5.87 %) was higher than that of the TFC-control (4.42 %), indicating that the unreacted PIP content in the PA layer was higher. The strong hydrogen bonding between the PVA-modified substrate and the PIP resulted in the substrate adsorbing a large amount of PIP, promoting the interfacial polymerization reaction, and hindering the diffusion of small molecule PIP, so that there were more unreacted PIP inside the PA layer [40], which reduced the consumption of TMC. The acyl chloride group on the TMC that did not participate in

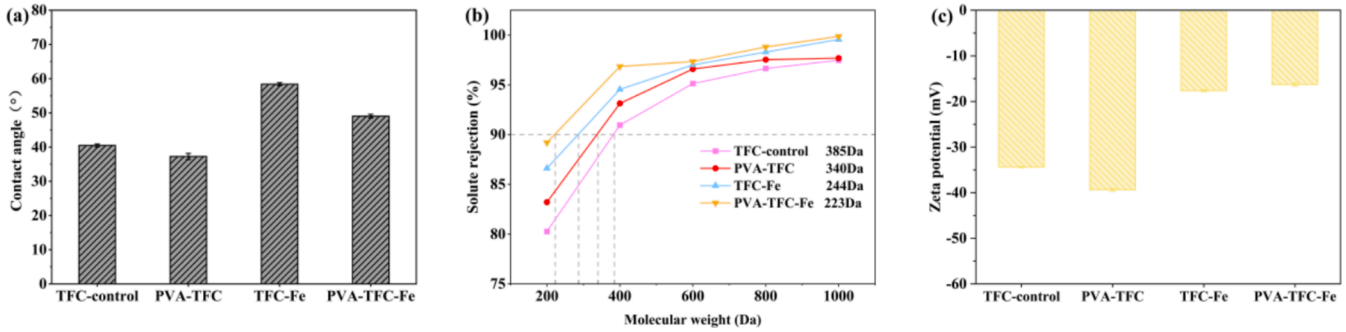

Fig. 5. **(a)** Contact angle of the membranes. **(b)** PEG rejections of the membranes. **(c)** Membrane surface zeta potential at neutral condition.

the reaction was subsequently hydrolyzed into a carboxyl functional group. As a result, the membrane surface contained more carboxyl functional groups. Furthermore, the increase in the proportion of carboxyl groups is beneficial to the deposition of Fe–TA polyphenol network, and the proportion of amide O = C–N groups on the surface of the PVA-TFC-Fe membrane(37.86 %) was significantly lower than that of the TFC-Fe membrane (46.2 %), indicating that the deposition density of Fe–TA polyphenol network was increased, which further confirmed that the more obvious Fe peak intensity on the surface of the PVA-TFC-Fe membrane was caused by the presence of more carboxyl functional groups on the membrane surface.

3.5. *Surface morphology and properties of the membranes*

To directly observe changes in the membrane surface morphology, the surface was characterized using SEM and AFM. As shown in Fig. 4**a-4d**, the surface of the TFC-control membrane was rough and contained nodules and firmly wrapped globules, which are typical morphologies formed by the reaction of small-molecule piperazine with acyl chloride through a PA cross-linked network [41]. Following the introduction of the PVA interlayer, a distinct crumpled morphology emerged on the surface of the PVA-TFC membrane, replacing the typical nodular morphology. This change can be attributed to the presence of hydroxyl functional groups in the hydrophilic PVA interlayer, which are capable of forming hydrogen bonds with PIP. This interaction slows down the diffusion rate of PIP and influences the reaction process of the PA layer, leading to the formation of crumpled morphology and reducing the thickness of the PA layer (**Fig. S3**). TFC-Fe membrane exhibited more pronounced granular and convex structures compared to the TFC-control membrane, indicating that abundant Fe–TA nanoparticles were deposited on the membrane surface and covered the pore structure, potentially reducing the membrane pore size and enhancing the selectivity to the target solutes [42]. In contrast to the TFC-Fe membrane, the PVA-TFC-Fe membrane showed obvious crumpled with dense granular morphology, resulting from the combined effect of interlayer and surface modification.

The membrane surface roughness was characterized using 3D AFM images. As shown in Fig. 4**e-4h**, the AFM characterizations were similar to those obtained from the surface SEM characterizations, the surface features of the membranes were also reflected in the AFM images. Furthermore, the average roughness (Ra) values are shown in **Fig. S4**. The TFC-control membrane has the lowest roughness (20.57 nm). However, after the Fe–TA polyphenol network coating, the roughness of the TFC-Fe membrane increased slightly, and its value was 28.52 nm. In contrast, the introduction of the PVA interlayer resulted in a distinct crumpled morphology on the membrane surface. The Ra value of the PVA-TFC membrane reached 41.63 nm. The crumpled morphology would increase the nano-voids between the substrate and the PA layer, which was beneficial to the improvement of permeability. Furthermore, the surface roughness of the PVA-TFC-Fe membrane exhibited the highest surface roughness, with a value of 61.27 nm. This could be attributed to the combined influence of the interlayer and the surface layer. Firstly, the introduction of the interlayer resulted in the formation of a rough surface on the PA layer. Secondly, the introduction of the interlayer altered the carboxyl content on the surface of the TFC membrane, which provided more chelation sites for Fe^{3+}, and more Fe–TA nanoparticles were deposited on the membrane surface, further increasing the membrane surface roughness.

Membrane hydrophilicity was evaluated by measuring the contact angles of the different TFC-NF membranes. As indicated in Fig. 5**a**, under neutral pH, the control membrane exhibited the lower contact angle of 40.5° among all the membranes. This result could be attributed to the hydrophilic carboxyl groups formed during the interfacial polymerization. The PVA-TFC membrane exhibited the lowest contact angle of 37.25° due to the membrane surface containing more hydrophilic carboxyl groups. However, when the Fe–TA layer was coated on the PA layer, the TFC-Fe and PVA-TFC-Fe membranes exhibited high contact angles of 58.4°and 49.05°, respectively. Similar to the results of Guo *et al.*[21], the current results indicate that the surface of the PA membrane had enhanced hydrophobic properties after coating, indicating that the coating layer might have a negative effect on the hydrophilicity of the membrane surface. The introduced Fe^{3+} chelated with the carboxyl groups on the membrane surface, which reduced the density of the hydrophilic carboxyl groups, a result that is in accordance with the FTIR results; hence, the hydrophilicity of the membrane decreased. Meanwhile, the chelation of Fe^{3+} and TA on the membrane surface formed dense metal − phenolic networks, which reduced the membrane pore size and further increased water transport resistance [43]. Therefore, the increase in water transport resistance was also responsible for the decrease in hydrophilicity. However, the PVA interlayer appeared to mitigate this effect, the PVA-TFC-Fe membrane showed a lower contact angle compared to the TFC-Fe membrane, indicating the sandwich structure reduces the resistance of water molecule diffusion, which is mainly manifested as the change of PA layer structure. Additionally, the hydrophilicity group in the interlayer is also beneficial to absorb water molecules from the surface of the PA separation layer and improve the diffusion of water molecules, thus improving the hydrophilicity of the membrane. Moreover, the responsiveness of the coating layer to pH will further affect the hydrophilicity [44].

The MWCO of the NF membrane was obtained by testing the rejection rate of neutral PEG with different molecular weights (200, 400, 600, 800, and 1000 Da) [45]. As shown in Fig. 5**b**, the control membrane had a MWCO of 385 Da. For the PVA-TFC, TFC-Fe and PVA-TFC-Fe membranes, the specific MWCO were 340, 244, and 223 Da, respectively, all of which have narrow pore sizes. The reduction in MWCO of the PVA-TFC membrane could be attributed to the introduction of hydrophilic PVA interlayer. Hydrogen bonding between the hydrophilic interlayer and PIP resulted in the substrate adsorbing more PIP, thereby controlling the diffusion rate during interfacial polymerization, which was conducive to the formation of more uniform pore size and reduced the defects of the PA layer. Therefore, the PVA-TFC membrane exhibits a lower MWCO. In contrast, the TFC-Fe membrane exhibited a lower

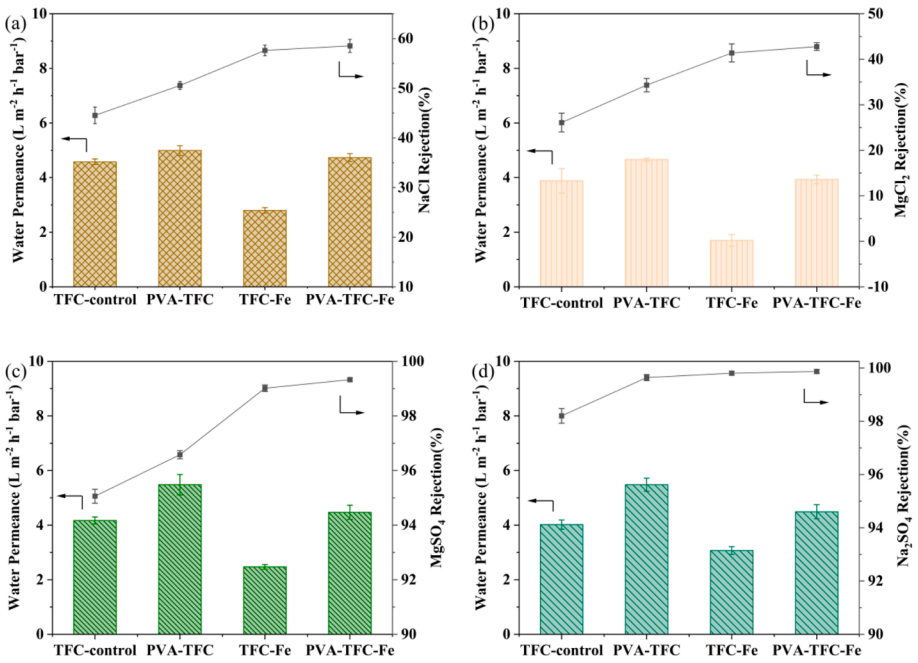

Fig. 6. Permeability and salt rejection of the membranes: **(a)** NaCl, **(b)** $MgCl_2$, **(c)** $MgSO_4$, and **(d)** Na_2SO_4 , and the concentration of each salt was 2000 mg/L.

MWCO, which indicated that the dense coating formed by the chelation of Fe^{3+} and TA molecules on the membrane surface could more effectively reduce the pore size of the membrane. For the PVA-TFC-Fe membrane, the PVA interlayer not only reduced the membrane pore size but also increased the carboxyl group content on the membrane surface, which provided additional chelation sites for Fe^{3+} and formed a denser Fe–TA coating. Consequently, the pore size of the membrane was further reduced. Combined FTIR, XPS and SEM characterizations revealed that the membrane surface was effectively coated, and the Fe^{3+} and TA molecules formed a dense Fe–TA layer on the membrane surface through chelation, which was the direct reason for the reduction in membrane pore size. The zeta potential test revealed that the PVA-TFC exhibited enhanced negative charge, demonstrating an increase in the proportion of carboxyl groups on the membrane surface again. However, the TFC-Fe and PVA-TFC-Fe membranes exhibited a lower negative charge surface than the control membrane(Fig. 5**c**) because increased positive charge was introduced to the membrane surface. The negative charge of the membrane surface gradually weakened, similar to what was observed for some of the features revealed by FTIR and XPS characterization.

3.6. Separation performance of the membranes

Four types of salt solutions, namely, Na_2SO_4, $MgSO_4$, $MgCl_2$, and NaCl, representing divalent and monovalent salts, were used to evaluate the separation performance of the membranes. Due to concentration polarization effects, the permeability of the salt solutions was lower than that of pure water for all membranes [46]. The rejection rate for sulfate was much higher than that for chloride ions, indicating that all membranes were negatively charged. Furthermore, the order of rejection of inorganic salts by traditional NF membranes is as follows: Na_2SO_4 > $MgSO_4$ > $MgCl_2$ > NaCl [47]. Differently, the order of desalination rate of NF membranes in this study is as follows: Na_2SO_4 > $MgSO_4$ > NaCl > $MgCl_2$. This could be due to the extremely negative charge phenomenon caused by the excessive hydrolysis of acyl chloride in the PIP-based membrane due to the addition of an acid acceptor in the aqueous phase [48,49], which resulted in the isoelectric point of the PIP-base membrane lower (**Fig. S5**). As shown in Fig. 6**b and 6c**. the $MgSO_4$ and Na_2SO_4 rejection rates of all the modified membranes were higher than 99 %. The PVA-TFC-Fe membrane exhibited optimal performance, with $MgSO_4$ and Na_2SO_4 rejection rates at 99.33 % and 99.87 %, respectively, which were better than the rejection rates of the control membrane. The enhanced rejection of sulfate by the modified membranes did not show excellent separation performance because of the negatively charged SO_4^{2-} ions could generate strong electrostatic repulsion with the negatively charged membrane surface, and the larger ionic radius of SO_4^{2-} (0.38 nm) [50].

However, compared with the rejection of large-sized sulfate, the rejection of small-sized inorganic salt (NaCl, $MgCl_2$) showed more interesting results. Fig. 6**a and 6b** present the separation performance of the modified membranes for two small-sized inorganic salts (NaCl and $MgCl_2$). The rejection rates of NaCl and $MgCl_2$ of the PVA-TFC membrane exhibited an increase of 6.03 % and 8.23 %, respectively, with a notable rise in water flux. and there was no obvious phenomenon that the enhancement of separation performance limited the permeability. The observed effects could be attributed to the following aspects: Firstly, the PVA interlayer affected the interfacial polymerization reaction, contributing to the formation of a defect-free morphology, improving the membrane surface cross-linking degree (**Fig. S6**), narrowing the membrane pore size, and enhancing carboxyl group content. This resulted in an improvement in separation performance, due to a combination of size exclusion and Donnan effects. Secondly, the interlayer facilitated the formation of a thin and crumpled PA separation layer, which provided less resistance and greater surface area for transporting water molecules. Furthermore, the increase in the content of hydrophilic functional groups resulted in more water molecules forming hydrogen bonds with them, which accelerated the transmission of water molecules. However, after surface Fe–TA coating modification, the carboxyl group on the membrane surface chelated with Fe^{3+}, which exerted an adverse effect on the negative charge and the removal of the monovalent ions of the Fe–TA-coated membranes. As a result, the separation performance of the TFC-Fe membrane was significantly improved, and the rejection rates of NaCl and $MgCl_2$ were increased by 13.09 % and 15.31 % respectively compared with the control membrane, and the pore size of the TFC-Fe membrane was much smaller than that of TFC-control, as evidenced by the pore size results. This finding indicates that the Donnan effect was not the key mechanism for NaCl and $MgCl_2$ rejections; instead, size exclusion played the dominant role in the rejection

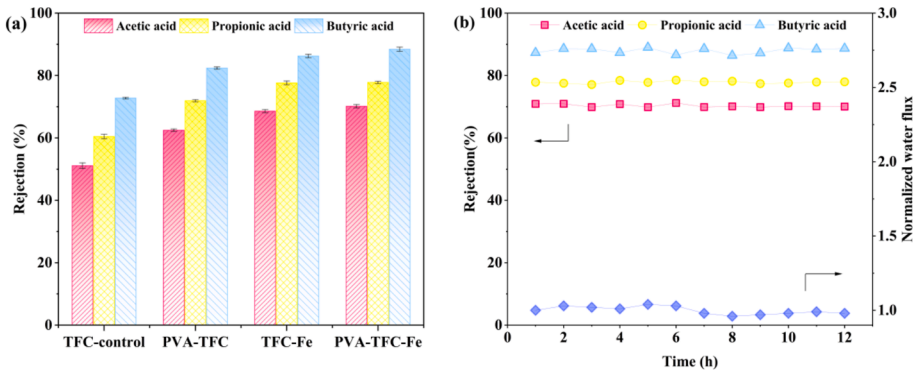

Fig. 7. (a) Rejections of the three VFAs by the membranes. **(b)** Stability of the long-term operation of the PVA-TFC-Fe membrane in mixed solutions of VFAs. The tests were conducted at 4 bar, pH 7.3, and 25 °C, and the concentration of each VFA was 2,000 mg/L.

of NaCl and $MgCl_2$. Hence, the presence of the Fe–TA coating layer substantially narrowed the effective pore diameter of the coated membranes, and the increased steric hindrance effect enhanced the entrapment of small-sized inorganic salts. For the PVA-TFC-Fe membrane, the introduction of the PVA interlayer not only narrowed the pore size but also provided more chelating sites for Fe^{3+} with the increase of carboxyl content. The compactness of the Fe–TA layer was further increased, and the optimal rejection rates of NaCl and $MgCl_2$ were obtained. In addition, the introduction of interlayer also mitigated the problem of permeability decline caused by the coating and had good permeability with high separation performance.

3.7. Membrane rejection performance and mechanism of the organic carbon source

The performance of the membranes in VFA recovery was investigated under neutral pH. As shown in Fig. 7**a**, the modified membranes exhibited increased rejections compared to the control membrane and the optimized retentions were achieved by the PVA-TFC-Fe membrane. This result confirmed the high separation performance of the PVA-TFC-Fe membrane, which is consistent with the conclusions drawn in the previous sections. Particularly, the TFC-control membrane had the lowest retention with rejection rates of 51.11 %, 60.47 %, and 72.77 % for acetic acid, propionic acid, and butyric acid, respectively. By contrast, the PVA-TFC-Fe membrane's rejection rates for acetic acid, propionic acid, and butyric acid were 70.16 %, 77.81 %, and 88.44 %, respectively, indicating that higher separation selectivity and 15.67 %–19.05 % rejection enhancement were achieved. Furthermore, the PVA-TFC-Fe membrane demonstrated stable VFA rejection and water flux during 12 h of continuous operation (Fig. 7**b**), revealing its good structural stability. This result is expected from NF mechanisms for VFA rejection, including the size exclusion and Donnan effects [51]. The conclusions in the previous sections show that the enhanced separation performance of the coated membranes was mainly due to the reduction in the membrane pore size. However, the electrostatic repulsion effect also played an important role. The pKa values of the VFAs used in this study were between 4.76 and 4.88 [52]. Under neutral pH conditions (pH > pKa), VFAs exist in the form of dissociated molecules ($R\text{-}COO^-$) and are easily dissolved. Some of the carboxyl groups on the surface of the coated membrane were chelated by Fe^{3+}, but the majority of the carboxyl groups were still distributed within the matrix of the PA layer [53]. Moreover, the PVA-TFC-Fe membrane still had anionic properties because of the carboxyl groups in the membrane under neutral pH conditions. As a result, electrostatic repulsion occurred, and VFAs were effectively rejected by the PVA-TFC-Fe membrane. In contrast, despite the surface of the PVA-TFC membrane containing more carboxyl functional groups, its separation performance is not as excellent as that of the PVA-TFC-Fe membrane. The difference in properties is mainly MWCO, so the size exclusion effect is still dominant in the separation performance.

4. Conclusions

In this work, a novel sandwich-structure TFC-NF membrane was synthesized via chemically bonding PVA forming the interlayer and deposition of the Fe–TA complex on the surface of the PA layer. The coating of the Fe–TA polyphenol network effectively enhanced the size repulsion and integrity of the PA layer, which enhanced the separation performance of the NF membrane. Furthermore, the PVA interlayer further promoted the interlayer interaction between the PA layer and the Fe–TA polyphenol coating, and facilitated the deposition of Fe–TA polyphenol network on the PA layer, thereby improving the separation efficiency. At the same time, the interlayer also optimized the water transport pathway, reducing the permeation loss caused by the deposition of Fe–TA polyphenol network. The cross-flow NF test showed that the water permeability was increased from 3.97 L $m^{-2}h^{-1}$ bar^{-1} for the TFC-Fe membrane to 6.21 L $m^{-2}h^{-1}$ bar^{-1} for the PVA-TFC-Fe membrane. Meanwhile, the PVA-TFC-Fe membrane has excellent separation performance, with the rejection of Na_2SO_4 reaching 99.87 %. In addition, the PVA-TFC-Fe membrane exhibited a notable enhancement in the rejection rate of small molecule organic carbon sources, including acetic acid, propionic acid, and butyric acid, with increases of 19.05 %, 17.34 %, and 15.67 %, respectively, in comparison to the control membrane. The results of this study not only deepen the understanding of NF membrane fabrication, performance and application in small-molecule carbon source recovery but also provide ideas for the resource utilization of wastewater treatment based on the concept of sustainability. Meanwhile, this work is also expected to promote the further development of NF membranes for high-concentration organic wastewater treatment and resource utilization.

CRediT authorship contribution statement

Xiujuan Hao: Supervision, Writing – review & editing, Funding acquisition, Conceptualization, Formal analysis, Methodology, Writing – original draft. **Yukai Hu:** Project administration, Writing – original draft, Data curation, Formal analysis, Validation, Conceptualization, Methodology. **Rijian Quan:** Project administration, Validation, Resources. **Xiayu Xu:** Validation, Resources, Project administration. **Xin Liu:** Investigation. **Yukun Li:** Investigation. **Jiayu Tian:** Supervision, Writing – review & editing, Formal analysis, Methodology.

Declaration of competing interest

The authors declare that they have no known competing financial interests or personal relationships that could have appeared to influence the work reported in this paper.

Acknowledgments

This work was supported by the National Natural Science Foundation of China (NNSFC, No. 52100049) and the Natural Science Foundation of Inner Mongolia Autonomous Region (NSFIMAR, No. 2021BS05019).

Appendix A. Supplementary data

Supplementary data to this article can be found online at https://doi.org/10.1016/j.seppur.2025.132047.

Data availability

Data will be made available on request.

References

[1] P.V. Nidheesh, A. Kumar, D. Syam Babu, J. Scaria, M. Suresh Kumar, Treatment of mixed industrial wastewater by electrocoagulation and indirect electrochemical oxidation, Chemosphere 251 (2020) 126437, https://doi.org/10.1016/j.chemosphere.2020.126437.
[2] L. Li, N. Sun, S. Peng, Q. Yang, P. Yang, H. Zhou, J. Ai, H. He, D. Wang, W. Zhang, Molecular insights into the degradation of organic matter from secondary swine wastewater effluent: A comparative study of advanced oxidation processes, Chem. Eng. J. (2024) 156761, https://doi.org/10.1016/j.cej.2024.156761.
[3] M. Zheng, Z. Hu, T. Liu, M. Sperandio, E.I.P. Volcke, Z. Wang, X. Hao, H. Duan, S. E. Vlaeminck, K. Xu, Z. Zuo, J. Guo, X. Huang, G.T. Daigger, W. Verstraete, M.C. M. Van Loosdrecht, Z. Yuan, Pathways to advanced resource recovery from sewage, Nat Sustain (2024), https://doi.org/10.1038/s41893-024-01423-6.
[4] X. Wu, Z. Yu, S. Yuan, A. Tawfik, F. Meng, An ecological explanation for carbon source-associated denitrification performance in wastewater treatment plants, Water Res. 247 (2023) 120762, https://doi.org/10.1016/j.watres.2023.120762.
[5] B. Luo, Utilization of liquor wastewater as a sustainable carbon source for enhanced nitrogen removal in aerobic granular sludge systems with varying operation conditions, J. Water Process Eng. 65 (2024) (2024) 105721, https://doi.org/10.1016/j.jwpe.2024.105721.
[6] X. Fu, R. Hou, P. Yang, S. Qian, Z. Feng, Z. Chen, F. Wang, R. Yuan, H. Chen, B. Zhou, Application of external carbon source in heterotrophic denitrification of domestic sewage: A review, Sci. Total Environ. 817 (2022) 153061, https://doi.org/10.1016/j.scitotenv.2022.153061.
[7] M.A.A. Rocha, Recovery of volatile fatty acids from water using medium-chain fatty acids and a cosolvent, Chem. Eng. Sci. 165 (2017) 74–80, https://doi.org/10.1016/j.ces.2017.02.014.
[8] P.S. Goh, K.C. Wong, A.F. Ismail, Membrane technology: A versatile tool for saline wastewater treatment and resource recovery, Desalination 521 (2022) 115377, https://doi.org/10.1016/j.desal.2021.115377.
[9] J.L. Van Puffelen, C. Brienza, I.C. Regelink, I. Sigurnjak, F. Adani, E. Meers, O. F. Schoumans, Performance of a full-scale processing cascade that separates agricultural digestate and its nutrients for agronomic reuse, Sep. Purif. Technol. 297 (2022) 121501, https://doi.org/10.1016/j.seppur.2022.121501.
[10] H. Zhang, Z. Yu, J. Wang, Z. Ke, L. Tong, X. Tang, L. Bai, H. Zhang, G. Li, H. Liang, A review of inland nanofiltration and reverse osmosis membrane concentrates management: Treatment, resource recovery and future development, Crit. Rev. Environ. Sci. Technol. (2024) 1–27, https://doi.org/10.1080/10643389.2024.2436161.
[11] Z. Chu, K. Chen, C. Xiao, D. Ji, H. Ling, M. Li, H. Liu, Improving pressure durability and fractionation property via reinforced PES loose nanofiltration hollow fiber membranes for textile wastewater treatment, J. Taiwan Inst. Chem. Eng. 108 (2020) 71–81, https://doi.org/10.1016/j.jtice.2019.12.009.
[12] A.W. Mohammad, Y.H. Teow, W.L. Ang, Y.T. Chung, D.L. Oatley-Radcliffe, N. Hilal, Nanofiltration membranes review: Recent advances and future prospects, Desalination 356 (2015) 226–254, https://doi.org/10.1016/j.desal.2014.10.043.
[13] N.N.R. Ahmad, W.L. Ang, Y.H. Teow, A.W. Mohammad, N. Hilal, Nanofiltration membrane processes for water recycling, reuse and product recovery within various industries: A review, J. Water Process Eng. 45 (2022) 102478, https://doi.org/10.1016/j.jwpe.2021.102478.
[14] Y. Liu, X. Wang, H. Yang, Y.F. Xie, X. Huang, Preparation of nanofiltration membranes for high rejection of organic micropollutants and low rejection of divalent cations, J. Membr. Sci. 572 (2019) 152–160, https://doi.org/10.1016/j.memsci.2018.11.013.
[15] Y. Gao, Y. Zhao, X. Wang, C. Tang, X. Huang, Modulating the asymmetry of the active layer in pursuit of nanofiltration selectivity via differentiating interfacial reactions of piperazine, Environ. Sci. Technol. 56 (2022) 14038–14047, https://doi.org/10.1021/acs.est.2c04124.
[16] S. Li, Y. Wan, S. Guo, J. Luo, Ferric ions mediated defects narrowing of graphene oxide nanofiltration membrane for robust removal of organic micropollutants, Chem. Eng. J. 411 (2021) 128587, https://doi.org/10.1016/j.cej.2021.128587.
[17] R. Dai, X. Wang, C.Y. Tang, Z. Wang, Dually charged MOF-based thin-film nanocomposite nanofiltration membrane for enhanced removal of charged pharmaceutically active compounds, Environ. Sci. Technol. 54 (2020) 7619–7628, https://doi.org/10.1021/acs.est.0c00832.
[18] Y. Liu, K. Wang, Z. Zhou, X. Wei, S. Xia, X. Wang, Y.F. Xie, X. Huang, Boosting the performance of nanofiltration membranes in removing organic micropollutants: trade-off effect, strategy evaluation, and prospective development, Environ. Sci. Technol. 56 (2022) 15220–15237, https://doi.org/10.1021/acs.est.2c06579.
[19] H. Guo, Y. Deng, Z. Yao, Z. Yang, J. Wang, C. Lin, T. Zhang, B. Zhu, C.Y. Tang, A highly selective surface coating for enhanced membrane rejection of endocrine disrupting compounds: Mechanistic insights and implications, Water Res. 121 (2017) 197–203, https://doi.org/10.1016/j.watres.2017.05.037.
[20] A. Ben-David, R. Bernstein, Y. Oren, S. Belfer, C. Dosoretz, V. Freger, Facile surface modification of nanofiltration membranes to target the removal of endocrine-disrupting compounds, J. Membr. Sci. 357 (2010) 152–159, https://doi.org/10.1016/j.memsci.2010.04.015.
[21] H. Guo, Z. Yao, Z. Yang, X. Ma, J. Wang, C.Y. Tang, A one-step rapid assembly of thin film coating using green coordination complexes for enhanced removal of trace organic contaminants by membranes, Environ. Sci. Technol. 51 (2017) 12638–12643, https://doi.org/10.1021/acs.est.7b03478.
[22] X. Zhu, X. Cheng, J. Xing, T. Wang, D. Xu, L. Bai, X. Luo, W. Wang, G. Li, H. Liang, In-situ covalently bonded supramolecular-based protective layer for improving chlorine resistance of thin-film composite nanofiltration membranes, Desalination 474 (2020) 114197, https://doi.org/10.1016/j.desal.2019.114197.
[23] D. Xu, X. Zhu, X. Luo, Y. Guo, Y. Liu, L. Yang, X. Tang, G. Li, H. Liang, MXene nanosheet templated nanofiltration membranes toward ultrahigh water transport, Environ. Sci. Technol. 55 (2) (2021) 1270–1278, https://doi.org/10.1021/acs.est.0c06835.
[24] X. Song, Y. Zhang, H.M. Abdel-Ghafar, E.A. Abdel-Aal, M. Huang, S. Gul, H. Jiang, Polyamide membrane with an ultrathin GO interlayer on macroporous substrate for minimizing internal concentration polarization in forward osmosis, Chem. Eng. J. 412 (2021) 128607, https://doi.org/10.1016/j.cej.2021.128607.
[25] M. Liu, W. Chen, J. Fu, A. Wang, M. Ding, L. Zhang, L. Han, L. Gao, Hyaluronic acid-modified nanofiltration membrane for ultrahigh water permeance and efficient rejection of PFASs, Process Saf. Environ. Protect. 166 (2022) 214–221, https://doi.org/10.1016/j.psep.2022.08.021.
[26] F. Xiao, H. Ge, Y. Wang, S. Bian, Y. Tong, C. Gao, G. Zhu, Novel thin-film composite membrane with polydopamine-modified polyethylene support and tannic acid-Fe^{3+} interlayer for forward osmosis applications, J. Membr. Sci. 642 (2022) 119976, https://doi.org/10.1016/j.memsci.2021.119976.
[27] X. Zhu, X. Cheng, X. Luo, Y. Liu, D. Xu, X. Tang, Z. Gan, L. Yang, G. Li, H. Liang, Ultrathin thin-film composite polyamide membranes constructed on hydrophilic poly(vinyl alcohol) decorated support toward enhanced nanofiltration performance, Environ. Sci. Technol. 54 (2020) 6365–6374, https://doi.org/10.1021/acs.est.9b06779.
[28] X. Zhu, Z. Yang, Z. Gan, X. Cheng, X. Tang, X. Luo, D. Xu, G. Li, H. Liang, Toward tailoring nanofiltration performance of thin-film composite membranes: Novel insights into the role of poly(vinyl alcohol) coating positions, J. Membr. Sci. 614 (2020) 118526, https://doi.org/10.1016/j.memsci.2020.118526.
[29] P. Cheng, Y. Liu, X. Wei, K. Fan, S. Xia, Distinct efficacies of interlayers in tailoring polyamide nanofiltration membrane performance for organic micropollutant removal: dependent on substrate characteristics, Environ. Sci. Technol. 58 (2024) 14022–14033, https://doi.org/10.1021/acs.est.4c04648.
[30] Q. Zhao, D.L. Zhao, L.Y. Ee, T.-S. Chung, S.B. Chen, In-situ coating of Fe-TA complex on thin-film composite membranes for improved water permeance in reverse osmosis desalination, Desalination 554 (2023) 116515, https://doi.org/10.1016/j.desal.2023.116515.
[31] W. Liu, L. Long, Z. Yang, L. Wang, Q. Gan, S. Zhou, P. Sarkar, H. Guo, C.Y. Tang, Enhancing the removal of organic micropollutants by nanofiltration membrane with Fe (III)–tannic acid interlayer: Mechanisms and environmental implications, Water Res. 245 (2023) 120623, https://doi.org/10.1016/j.watres.2023.120623.
[32] S. Shao, F. Zeng, L. Long, X. Zhu, L.E. Peng, F. Wang, Z. Yang, C.Y. Tang, Nanofiltration membranes with crumpled polyamide films: a critical review on mechanisms, performances, and environmental applications, Environ. Sci. Technol. 56 (2022) 12811–12827, https://doi.org/10.1021/acs.est.2c04736.
[33] Y. Hu, F. Wang, Z. Yang, C.Y. Tang, Modeling nanovoid-enhanced water permeance of thin film composite membranes, J. Membr. Sci. 675 (2023) 121555, https://doi.org/10.1016/j.memsci.2023.121555.
[34] Y. Tang, L. Cheng, T. Wu, Z. Xu, Quantitative analysis of the influence of PVA interlayer on the permeation resistance of TFC NF membranes, Desalination 584 (2024) 117752, https://doi.org/10.1016/j.desal.2024.117752.
[35] Y. Liu, L. Bai, X. Zhu, D. Xu, G. Li, H. Liang, M.R. Wiesner, The role of carboxylated cellulose nanocrystals placement in the performance of thin-film composite (TFC) membrane, J. Membr. Sci. 617 (2021) 118581, https://doi.org/10.1016/j.memsci.2020.118581.
[36] Y. Li, X. You, R. Li, Y. Li, C. Yang, M. Long, R. Zhang, Y. Su, Z. Jiang, Loosening ultrathin polyamide nanofilms through alkali hydrolysis for high-permselective nanofiltration, J. Membr. Sci. 637 (2021) 119623, https://doi.org/10.1016/j.memsci.2021.119623.
[37] C.N.R. Rao, S. Natarajan, R. Vaidhyanathan, Metal carboxylates with open architectures, ChemInform 35 (2004) chin.200422252, https://doi.org/10.1002/chin.200422252.
[38] X. Zhu, H. Liang, X. Tang, L. Bai, X. Zhang, Z. Gan, X. Cheng, X. Luo, D. Xu, G. Li, Supramolecular-based regenerable coating layer of a thin-film composite nanofiltration membrane for simultaneously enhanced desalination and antifouling properties, ACS Appl. Mater. Interfaces 11 (2019) 21137–21149, https://doi.org/10.1021/acsami.9b03761.
[39] V.T. Do, C.Y. Tang, M. Reinhard, J.O. Leckie, Degradation of polyamide nanofiltration and reverse osmosis membranes by hypochlorite, Environ. Sci. Technol. 46 (2012) 852–859, https://doi.org/10.1021/es203090y.

[40] C. Jiang, L. Tian, Z. Zhai, Y. Shen, W. Dong, M. He, Y. Hou, Q.J. Niu, Thin-film composite membranes with aqueous template-induced surface nanostructures for enhanced nanofiltration, J. Membr. Sci. 589 (2019) 117244, https://doi.org/10.1016/j.memsci.2019.117244.
[41] Y. Liu, Y. Zhao, X. Wang, X. Wen, X. Huang, Y.F. Xie, Effect of varying piperazine concentration and post-modification on prepared nanofiltration membranes in selectively rejecting organic micropollutants and salts, J. Membr. Sci. 582 (2019) 274–283, https://doi.org/10.1016/j.memsci.2019.04.018.
[42] J. Lin, Q. Chen, R. Liu, W. Ye, P. Luis, B. Van der Bruggen, S. Zhao, Sustainable management of landfill leachate concentrate via nanofiltration enhanced by one-step rapid assembly of metal-organic coordination complexes, Water Res. 204 (2021) 117633, https://doi.org/10.1016/j.watres.2021.117633.
[43] S. Liu, X. Tong, S. Liu, D. An, J. Yan, Y. Chen, J. Crittenden, Multi-functional tannic acid (TA)-Ferric complex coating for forward osmosis membrane with enhanced micropollutant removal and antifouling property, J. Membr. Sci. 626 (2021) 119171, https://doi.org/10.1016/j.memsci.2021.119171.
[44] C. Liu, M. Yan, K. Guo, Y. Gao, F. Liu, B. Gao, Ta-Fe in-situ coating PES membrane and its application in oily wastewater treatment: Insight into modification and anti-fouling mechanisms, Sep. Purif. Technol. 346 (2024) 127506, https://doi.org/10.1016/j.seppur.2024.127506.
[45] M. Liu, Q. Chen, K. Lu, W. Huang, Z. Lü, C. Zhou, S. Yu, C. Gao, High efficient removal of dyes from aqueous solution through nanofiltration using diethanolamine-modified polyamide thin-film composite membrane, Sep. Purif. Technol. 173 (2017) 135–143, https://doi.org/10.1016/j.seppur.2016.09.023.
[46] Z. Wang, Z. Wang, S. Lin, et al., Nanoparticle-templated nanofiltration membranes for ultrahigh performance desalination, Nat Commun 9 (2018) 2004, https://doi.org/10.1038/s41467-018-04467-3.
[47] M.J.T. Raaijmakers, N.E. Benes, Current trends in interfacial polymerization chemistry, Prog. Polym. Sci. 63 (2016) 86–142, https://doi.org/10.1016/j.progpolymsci.2016.06.004.
[48] K. Wang, X. Wang, B. Januszewski, Y. Liu, D. Li, R. Fu, M. Elimelech, X. Huang, Tailored design of nanofiltration membranes for water treatment based on synthesis–property–performance relationships, Chem. Soc. Rev. 51 (2022) 672–719, https://doi.org/10.1039/D0CS01599G.
[49] L. Zhou, S. Gu, F. Xu, J. Zhang, Z. Hu, S. Li, Z. Xu, Ultrathin cyclodextrin-based nanofiltration membrane with tunable microporosity for antibiotic desalination, J. Membr. Sci. 715 (2025) 123504, https://doi.org/10.1016/j.memsci.2024.123504.
[50] A. Al-Nahari, S. Li, B. Su, Negatively charged nanofiltration membrane with high performance via the synergetic effect of benzidinedisulfonic acid and trimethylamine during interfacial polymerization, Sep. Purif. Technol. 291 (2022) 120947, https://doi.org/10.1016/j.seppur.2022.120947.
[51] X. Zhu, A. Leininger, D. Jassby, N. Tsesmetzis, Z.J. Ren, Will membranes break barriers on volatile fatty acid recovery from anaerobic digestion? ACS EST Eng. 1 (2021) 141–153, https://doi.org/10.1021/acsestengg.0c00081.
[52] M.N. Pervez, A. Mahboubi, C. Uwineza, T. Zarra, V. Belgiorno, V. Naddeo, M. J. Taherzadeh, Factors influencing pressure-driven membrane-assisted volatile fatty acids recovery and purification-A review, Sci. Total Environ. 817 (2022) 152993, https://doi.org/10.1016/j.scitotenv.2022.152993.
[53] X. Li, X. Chen, C.H. Loh, K. Fu, L. Yang, A novel in-situ hydrolysis approach to prepare ultra-selective and ultrasmooth nanofiltration membrane for efficient and sustainable ion separation, J. Membr. Sci. 694 (2024) 122433, https://doi.org/10.1016/j.memsci.2024.122433.